Solid State Sciences 23 (2013) 88–95

Contents lists available at SciVerse ScienceDirect

Solid State Sciences

journal homepage: www.elsevier.com/locate/ssscie

Light-induced structural changes in $(HgBr_2)_3(As_4S_4)_2$: An X-ray single-crystal diffraction, Raman spectroscopy and *ab initio* study

M. Zoppi [a], L. Bindi [a], T. Rödl [b], F. Pielnhofer [b], R. Weihrich [b], A. Pfitzner [b], P. Bonazzi [a,*]

[a] Dipartimento di Scienze della Terra, Università di Firenze, via La Pira 4, I-50121 Firenze, Italy
[b] Institut für Anorganische Chemie, Universität Regensburg, Universitätsstrasse 31, D-93040 Regensburg, Germany

ARTICLE INFO

Article history:
Received 18 April 2013
Received in revised form
11 June 2013
Accepted 15 June 2013
Available online 25 June 2013

Keywords:
X-ray single-crystal diffraction
Raman spectroscopy
Realgar-type As_4S_4 molecule
Pararealgar-type As_4S_4 molecule
Photo-induced solid-state isomerization
Ab initio band structure calculations

ABSTRACT

To investigate the behaviour of the As_4S_4 molecule within a crystal-chemical environment differing from realgar, α-As_4S_4, and its high-temperature polymorph, β-As_4S_4, the effects of the light exposure on the structure of the $(HgBr_2)_3(As_4S_4)_2$ adduct have been studied. Differently from the cases previously studied, the action of the light filtered using a 550 nm long-wavelength pass filter did not produce any evident effect on the unit-cell. On the other hand, employing the 440 nm long-wavelength pass filter, remarkable variations of the unit-cell parameters were observed. In particular, an increase of the *a*, *c*, and β, and a decrease of the *b* parameter, producing on the whole an expansion of the unit-cell volume, is observed as a function of the light exposure times. Structure refinements indicated that the increase of the unit-cell volume is to ascribe to the formation of an increasing fraction (up to 20%) of pararealgar-type replacing the realgar-type molecule. Further light-exposure did not cause any further increase of the lattice parameters. On the contrary, a decrease of the unit-cell volume occurred by keeping the crystal in the dark (46 days): due to the loss of the crystallinity, only the core of the crystal, less altered and with smaller unit-cell volume, contributes to the diffraction effects. Micro-Raman spectra were collected on crystals exposed to the above mentioned wavelength light for increasing times. The peak at 275(±1) cm^{-1} whose intensity increases as a function of the exposure time confirms the transition from a realgar- to a pararealgar-type molecule in the $(HgBr_2)_3(As_4S_4)_2$ adduct. Relativistic DFT-GGA *ab initio* band structure calculations reveal a direct band gap of 2.04 eV and quite flat valence and conduction bands around the Fermi level. According to analyses of the atomic orbital contributions to the electronic band structures the highest occupied states are attributed to non-bonding *p*-states of As.

1. Introduction

Molecular arsenic sulphides, as well as bulk glasses and thin films in the As–S system, are of interest to physicists and material scientists and are widely studied for their potential or actual application in optics and optoelectronics, mainly because of reversible and/or irreversible photo-induced changes of their physico-chemical properties e.g. [1,2]. In particular, the mineral realgar, α-As_4S_4 [3], and its high-temperature polymorph, β-As_4S_4 [4], irreversibly transform into its isomer pararealgar [5,6] when exposed to visible light [7–15]. According to a model first proposed by Bindi et al. [16] and subsequently elaborated by Kyono et al. [9] and Naumov et al. [13,14], the photo-induced solid-state isomerization of the realgar-type (*r*-type) to pararealgar (*p*-type) As_4S_4 molecule occurs through a self-sustainable mechanism based on initial aerobic photo-oxidation [$5As_4S_4$ (*r*-type) + $3O_2$ + $h\nu$ → $4As_4S_5$ + $2As_2O_3$] followed by release of a S atom by breaking an As–S–As linkage to form pararealgar: As_4S_5 → As_4S_4 (*p*-type) + S. Propagation of the process could cyclically occur by re-attachment of the free S to another realgar-type As_4S_4 molecule: As_4S_4 (*r*-type) + S → As_4S_5 and subsequent formation of pararealgar As_4S_5 → As_4S_4 (*p*-type) + S. As Naumov et al. [13,14] pointed out, the first step of this reaction requires photo-excitation ('light stage'), whereas the second one represents a self-accelerated solid-state chain reaction which does not need the exposure to light ('dark stage').

It is not clear which main factors may affect the kinetics of the autocatalytically induced conversion ('dark stage') and what determines the amount of As_4S_5 molecules which can be stored within the structure: it is a fact, however, that different compounds containing *r*-type As_4S_4 molecules show different routes of transformation. A common feature for all of them is an expansion of the unit-cell volume, which was interpreted as a

* Corresponding author. Tel.: +39 (0)55 2757532.
E-mail address: paola.bonazzi@unifi.it (P. Bonazzi).

1293-2558/$ – see front matter © 2013 Elsevier Masson SAS. All rights reserved.
http://dx.doi.org/10.1016/j.solidstatesciences.2013.06.007

consequence of the increment in the number of the As_4S_5 molecules in light-exposed β-As_4S_{4+x} crystals [11] and, to much lesser extent, in realgar [9,14], even without formation of detectable amounts of arsenolite. To investigate the transformation from the *r*- to *p*-type molecules within a crystal-chemical environment differing from α-As_4S_4 and β-As_4S_4, Bonazzi et al. [17] studied by single-crystal XRD and Raman spectroscopy the effects of the light exposure on the structure of the $(HgI_2)(As_4S_4)$ adduct, consisting of a packing of nearly linear HgI_2 molecules and As_4S_4 cage-molecules [18]. Although a marked increase of the unit-cell volume was observed as a function of the exposure time, no significant amounts of As_4S_5 molecule were observed at any step of the alteration process and the increase of the unit-cell volume was ascribed to the formation of an increasing fraction (up to 59%) of *r*-type molecules replaced by *p*-type molecules which, indeed, exhibit a greater molecular volume [19]. Similarly, Zoppi and Pratesi [15] demonstrated that when the exposure to light is done under anaerobic conditions, β-As_4S_4 transforms to para-realgar without evidence of formation of As_4S_5 molecules within the structure nor of crystallization of arsenolite. The reverse transformation, from pararealgar to β-As_4S_4 and realgar, is also possible and occurs by heating pararealgar in vacuum within the stability field of realgar [7,15].

From the previous literature becomes evident that the transformation from *r*- to *p*-type molecules occurs through different routes depending on the presence or the absence of air during the process of alteration [15], the kind of molecular packing as well as the kind of molecules combined together in the structure [11,17].

The aim of the present paper is to investigate by single-crystal XRD and Raman spectroscopy the response to light exposure of the As_4S_4 molecule within the structure of the $(HgBr_2)_3(As_4S_4)_2$ adduct [20]. The crystal structure of $(HgBr_2)_3(As_4S_4)_2$ [$a = 9.593(5)$, $b = 11.395(5)$, $c = 13.402(5)$ Å, $\beta = 107.27(3)^\circ$, $V = 1399(1)$ Å^3, $Z = 2$; space group $P2_1/c$], indeed, consists of a packing of linear and slightly bent $HgBr_2$ molecules and undistorted As_4S_4 cage-molecules, quite similar to those found in realgar, β-As_4S_4 and alacranite [21]. The experimental findings are correlated with the results of relativistic DFT-GGA calculations of the electronic band structure of the title compound.

Table 1
Unit-cell parameters of the $(HgBr_2)_3(As_4S_4)_2$ adduct (crystal A) measured after different times of exposure to filtered visible light.

Time (min)	a (Å)	*b* (Å)	*c* (Å)	*β* (°)	Vol (Å^3)
550 nm long pass filter					
0	9.559(7)	11.441(3)	13.397(5)	106.96(4)	1401(1)
40	9.565(7)	11.442(3)	13.394(5)	106.97(4)	1402(1)
100	9.560(8)	11.439(3)	13.399(6)	106.96(4)	1401(1)
180	9.560(7)	11.440(3)	13.396(5)	106.97(3)	1401(1)
240	9.561(7)	11.436(3)	13.398(5)	106.96(4)	1401(1)
360	9.562(6)	11.441(2)	13.397(4)	106.98(3)	1401(1)
420	9.563(7)	11.440(3)	13.399(5)	107.01(4)	1401(1)
440 nm- long pass filter					
0	9.563(7)	11.440(3)	13.399(5)	107.01(4)	1401(1)
60	9.606(9)	11.406(4)	13.410(7)	107.22(5)	1403(2)
180	9.71(1)	11.333(5)	13.442(9)	107.94(7)	1406(2)
240	9.756(9)	11.326(3)	13.472(6)	108.43(4)	1412(2)
300	9.77(1)	11.321(4)	13.499(7)	108.57(5)	1415(2)
360	9.78(2)	11.337(6)	13.49(1)	108.61(8)	1418(3)
420	9.785(6)	11.335(2)	13.511(5)	108.78(3)	1418(1)
480	9.791(2)	11.346(2)	13.517(5)	108.88(3)	1420(1)

2. Experimental

2.1. Synthesis

Yellow single crystals of $(HgBr_2)_3(As_4S_4)_2$ can be synthesized either by reaction of stoichiometric amounts of $HgBr_2$, As, and S at elevated temperature or by reaction of a stoichiometric mixture of $HgBr_2$ and As_4S_4 in CS_2 at 160 °C for two weeks. The solvo-thermal route resulted in $(HgBr_2)_3(As_4S_4)_2$ as the major product and $Hg_3S_2Br_2$ as main byproduct. Crystals of a higher quality are obtained in case of the solvent free high-temperature reaction but these are the minor reaction product, see Ref. [20] for details. The crystals for the present study were obtained from such solvent free reactions.

Table 2
Experimental details of data collection and structure refinement of the $(HgBr_2)_3(As_4S_4)_2$ adduct (crystal B) exposed to the 440-nm-filtered light.

	(a)	(b)	(c)	(d)	(e)
Space group	$P2_1/c$	$P2_1/c$	$P2_1/c$	$P2_1/c$	$P2_1/c$
Cell parameters					
a (Å)	9.5324(5)	9.6199(5)	9.7524(5)	9.7542(8)	9.651(3)
b (Å)	11.4114(4)	11.3453(5)	11.2876(5)	11.3161(8)	11.369(1)
c (Å)	13.3794(6)	13.4074(7)	13.4775(7)	13.482(1)	13.417(3)
β (°)	106.974(5)	107.538(6)	108.655(6)	108.783(9)	107.86(3)
V (Å^3)	1392.0(1)	1395.3(3)	1405.7(3)	1408.8(5)	1401(1)
θ-range (°)	4.2–30.5	4.3–30.6	4.2–30.6	4.2–30.8	4.2–24.9
Range of *h*,*k*,*l*	$-13 \le h \le 8$	$-7 \le h \le 13$	$-13 \le h \le 7$	$-7 \le h \le 13$	$-8 \le h \le 11$
	$-7 \le k \le 15$	$-15 \le k \le 13$	$-15 \le k \le 13$	$-15 \le k \le 15$	$-9 \le k \le 12$
	$-10 \le l \le 18$	$-18 \le l \le 18$	$-18 \le l \le 19$	$-18 \le l \le 19$	$-13 \le l \le 9$
Scan mode	φ/ω	φ/ω	φ/ω	φ/ω	φ/ω
Exposure time per frame (s)	30	80	100	108	120
Frame width (°)	1	1	1	1	1
Detector to sample dist. (mm)	45	45	45	45	45
Number of parameters	115	115	124	129	115
Collected reflections	6989	6668	6795	6801	3664
Independent reflections	3724	3695	3710	3726	1792
Refl. with $F_0 > 4\sigma(F_0)$	2055	2325	2094	1819	613
R_{int} (%)	5.75	3.33	3.52	5.42	14.07
R_{obs} (%)	5.24	4.87	6.33	6.86	12.01
$\Delta\rho_{max}$ (eÅ^{-3})	1.65	1.40	1.92	1.54	1.34
$\Delta\rho_{min}$ (eÅ^{-3})	−2.05	−1.51	−1.07	−1.28	−1.10

Notes: (a) = unaltered crystal; (b, c, d) = crystal exposed to filtered light (>440 nm) for 180, 420, and 600 min, respectively; (e) = crystal kept in the dark (46 days) after light-induced alteration.

Table 3
Fractional atomic coordinates, site occupancy factors (s.o.f.), and equivalent displacement parameters for the $(HgBr_2)_3(As_4S_4)_2$ crystal (B) at different steps of alteration.

	x/a	y/b	z/c	s.o.f.	U_{eq}
(a)					
Hg1	0	0.5	0.5	1	0.0595(3)
Hg2	0.7615(1)	0.2195(1)	0.6941(1)	1	0.0621(2)
Br1	0.2194(1)	0.6247(1)	0.5561(1)	1	0.0417(4)
Br2	0.8543(2)	0.0298(1)	0.6657(1)	1	0.0498(4)
Br3	0.7506(2)	0.4256(1)	0.7332(1)	1	0.0545(4)
As1	0.3738(2)	0.0786(1)	0.5807(1)	1	0.0372(3)
As2	0.1193(2)	0.1720(1)	0.5205(1)	1	0.0358(3)
As3	0.3911(2)	0.3683(1)	0.5016(1)	1	0.0347(3)
As4	0.3719(2)	0.3577(1)	0.6895(1)	1	0.0340(3)
S1	0.1394(4)	0.2957(3)	0.6536(2)	1	0.0361(8)
S2	0.4905(4)	0.1926(3)	0.4933(3)	1	0.0398(8)
S3	0.4632(4)	0.1767(3)	0.7308(2)	1	0.0375(8)
S4	0.1660(4)	0.3086(3)	0.4141(2)	1	0.0378(8)
(b)					
Hg1	0	0.5	0.5	1	0.0626(3)
Hg2	0.7641(1)	0.2233(1)	0.6957(1)	1	0.0668(2)
Br1	0.2163(1)	0.6269(1)	0.5534(1)	1	0.0471(3)
Br2	0.8509(2)	0.0318(1)	0.6663(1)	1	0.0577(4)
Br3	0.7540(2)	0.4293(1)	0.7359(1)	1	0.0632(4)
As1	0.3770(1)	0.0780(1)	0.5811(1)	1	0.0418(3)
As2	0.1226(1)	0.1691(1)	0.5227(1)	1	0.0410(3)
As3	0.3891(1)	0.3691(1)	0.5010(1)	1	0.0416(3)
As4	0.3744(1)	0.3586(1)	0.6895(1)	1	0.0385(3)
S1	0.1447(3)	0.2951(3)	0.6551(2)	1	0.0407(7)
S2	0.4896(3)	0.1938(3)	0.4922(2)	1	0.0436(7)
S3	0.4680(3)	0.1779(3)	0.7313(2)	1	0.0426(7)
S4	0.1636(3)	0.3063(3)	0.4140(2)	1	0.0433(7)
(c)					
Hg1	0	0.5	0.5	1	0.0724(4)
Hg2	0.7700(1)	0.2309(1)	0.6993(1)	1	0.0777(3)
Br1	0.2107(2)	0.6305(2)	0.5486(1)	1	0.0597(5)
Br2	0.8447(2)	0.0353(2)	0.6681(2)	1	0.0736(6)
Br3	0.7612(3)	0.4364(2)	0.7412(2)	1	0.0853(7)
As1	0.3826(2)	0.0777(2)	0.5817(1)	1	0.0536(5)
As2	0.1281(2)	0.1639(2)	0.5264(1)	1	0.0524(5)
As3	0.3846(2)	0.3709(2)	0.4992(2)	0.868(6)	0.0492(7)
As4	0.3799(2)	0.3587(2)	0.6909(1)	1	0.0504(4)
S1	0.1540(4)	0.2939(4)	0.6572(3)	1	0.051(1)
S2	0.4879(5)	0.1964(5)	0.4915(4)	0.868	0.050(1)
S3	0.4767(5)	0.1773(4)	0.7315(3)	1	0.055(1)
S4	0.1599(5)	0.3003(5)	0.4141(3)	1	0.061(1)
As3b	0.366(2)	0.227(1)	0.449(1)	0.132	0.064(6)
S2b	0.448(5)	0.385(4)	0.558(4)	0.132	0.07(1)
(d)					
Hg1	0	0.5	0.5	1	0.0800(4)
Hg2	0.7717(1)	0.2320(1)	0.7000(1)	1	0.0841(4)
Br1	0.2096(2)	0.6308(2)	0.5477(2)	1	0.0687(6)
Br2	0.8431(3)	0.0362(2)	0.6688(2)	1	0.0818(7)
Br3	0.7633(3)	0.4366(2)	0.7426(2)	1	0.0960(8)
As1	0.3838(2)	0.0777(2)	0.5819(2)	1	0.0597(5)
As2	0.1290(2)	0.1630(2)	0.5269(1)	1	0.0588(5)
As3	0.3849(3)	0.3705(2)	0.4992(2)	0.848(6)	0.0564(8)
As4	0.3809(2)	0.3579(2)	0.6918(2)	0.956(6)	0.0541(7)
S1	0.1549(5)	0.2928(5)	0.6571(3)	0.956	0.054(1)
S2	0.4891(6)	0.1971(5)	0.4928(4)	0.848	0.056(1)
S3	0.4772(5)	0.1771(4)	0.7322(3)	1	0.059(1)
S4	0.1580(6)	0.2971(6)	0.4139(3)	1	0.072(2)
As3b	0.365(1)	0.227(1)	0.448(1)	0.152	0.061(5)
S2b	0.459(7)	0.397(6)	0.568(6)	0.152	0.12(2)
As4b	0.282(5)	0.283(5)	0.695(4)	0.044	0.07(2)
(e)					
Hg1	0	0.5	0.5	1	0.092(2)
Hg2	0.7665(4)	0.2255(3)	0.6973(3)	1	0.095(2)
Br1	0.3786(8)	0.0772(6)	0.5811(6)	1	0.067(3)
Br2	0.1238(8)	0.1676(6)	0.5240(6)	1	0.062(3)
Br3	0.3868(8)	0.3688(6)	0.5015(7)	1	0.075(3)
As1	0.3758(8)	0.3570(6)	0.6915(6)	1	0.066(3)
As2	0.2134(8)	0.6273(6)	0.5514(7)	1	0.080(3)
As3	0.8499(8)	0.0338(6)	0.6672(7)	1	0.084(3)
As4	0.7573(9)	0.4303(7)	0.7389(7)	1	0.093(3)
S1	0.146(2)	0.292(2)	0.656(2)	1	0.069(6)
S2	0.488(2)	0.193(2)	0.492(2)	1	0.067(6)
S3	0.468(2)	0.175(2)	0.731(2)	1	0.062(6)
S4	0.160(2)	0.303(2)	0.417(2)	1	0.075(7)

Notes: (a) = unaltered crystal; (b, c, d) = crystal exposed to filtered light (>440 nm) for 180, 420, and 600 min, respectively; (e) = crystal kept in the dark (46 days) after light-induced alteration.

2.2. X-ray diffraction

Three well shaped tabular crystals of $(HgBr_2)_3(As_4S_4)_2$ (labelled A, B, and C) were selected under a microscope from the run product. Crystal A, chosen to study the variation of the unit-cell parameters as a function of the light exposure, was mounted on a Bruker Mach3 diffractometer and the unit-cell values were initially determined before any exposure to light by centring 25 relatively strong reflections ($9 < \theta < 13°$). The crystal was then exposed to filtered visible light using a 550-nm long-wavelength pass filter (yellow) like in the photo-induced alteration experiments previously carried out [8,11,17]; after each light exposure, unit-cell parameters were determined (Table 1). The same procedure was repeated using a 440-nm long-wavelength pass filter (green) as long as it was still possible to centre the same set of reflections (Table 1). After 480 min of light exposure, probably also because of the hygroscopic nature of this adduct, crystal A underwent a sudden deterioration. For this reason, before starting light-exposure experiment on a second crystal (B), it was coated with hydro-repellent glue (methyl-2-cyanoacrylate). Intensity data were collected from crystal B on a CCD-equipped Oxford Diffraction Xcalibur3 diffractometer (Mo$K\alpha$ radiation) fitted with a Sapphire 2 CCD detector for the most significant steps of the alteration chosen on the basis of the alteration path observed for crystal A (see Table 2 for details). Intensity integration and standard Lorentz-polarization correction were performed with the *CrysAlis* RED [22] software package. The

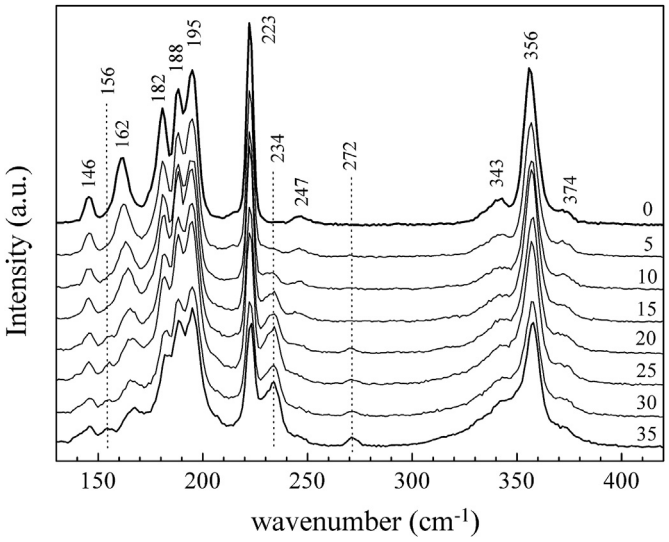

Fig. 1. Raman spectrum of the unaltered crystal of $(HgBr_2)_3(As_4S_4)_2$ (crystal C) together with those collected every 5 min of exposure to filtered light (440 nm long-wavelength pass filter). The intensity of the bands ascribed to the pararealgar molecule (156, 234 and 272 cm^{-1}) are marked with the dashed lines. At 182, 188, 195, 223 and 356 cm^{-1} the strongest bands of the $(HgBr_2)_3(As_4S_4)_2$ adduct.

program ABSPACK in *CrysAlis* RED [22] was used for the absorption correction. After 600 min of exposition to the 440-nm-filtered light, crystal B was kept in the dark for 46 days and then XRD data were collected again. Structure refinements were performed on F^2 using the SHELXL-97 program [23]. Neutral scattering curves for As, S, Hg and Br were taken from the *International Tables for X-ray Crystallography* [24]. Isotropic full-matrix least–squares cycles were initially run starting from the structural data published by Bräu and Pfitzner [20] and assuming the atom sites as fully occupied. After alteration, structural models involving partial occupancy of some atoms and additional atoms were refined. In particular, after 420 min of exposure to light (Table 2, column c), the unusually high value of the isotropic displacement factor for S2 and As3 strongly suggested partial occupancy at these sites. Accordingly, examination of the Δ*F*-Fourier map revealed the presence of two residual peaks (*i.e.*, As3b and S2b, respectively). The occupancy factors of As3 and S2 resulted close to a common value (k), while the occupancy factor for As3b and S2b resulted approximately equal to $1 - k$. Therefore, in order to reduce the number of free variables and to obtain a reliable model, only one parameter (k) was refined to constrain occ.(As3) = occ.(S2) = k, and occ.(As3b) = occ.(S2b) = $1 - k$. The atomic set obtained for step (c) was used as a starting model for the refinement of the intensity data collected at the step (d); however, a further residual electron density peak close to As4 was found. This was assigned to a further arsenic atom (As4b), supposed to be the evidence of a newly formed *p*-type molecule with a different orientation, even if no evidence of residual peaks to be assigned to S atoms of the new *p*-type molecule was detected. The sum of its site occupancy factor and that of As4 were constrained to sum up to one. The site occupancy factor of S1 was constrained to that of As4, having the former atom a too short distance from As4b (1.19 Å). Final atomic parameters obtained with anisotropic full-matrix least–squares cycles are reported in Table 3.

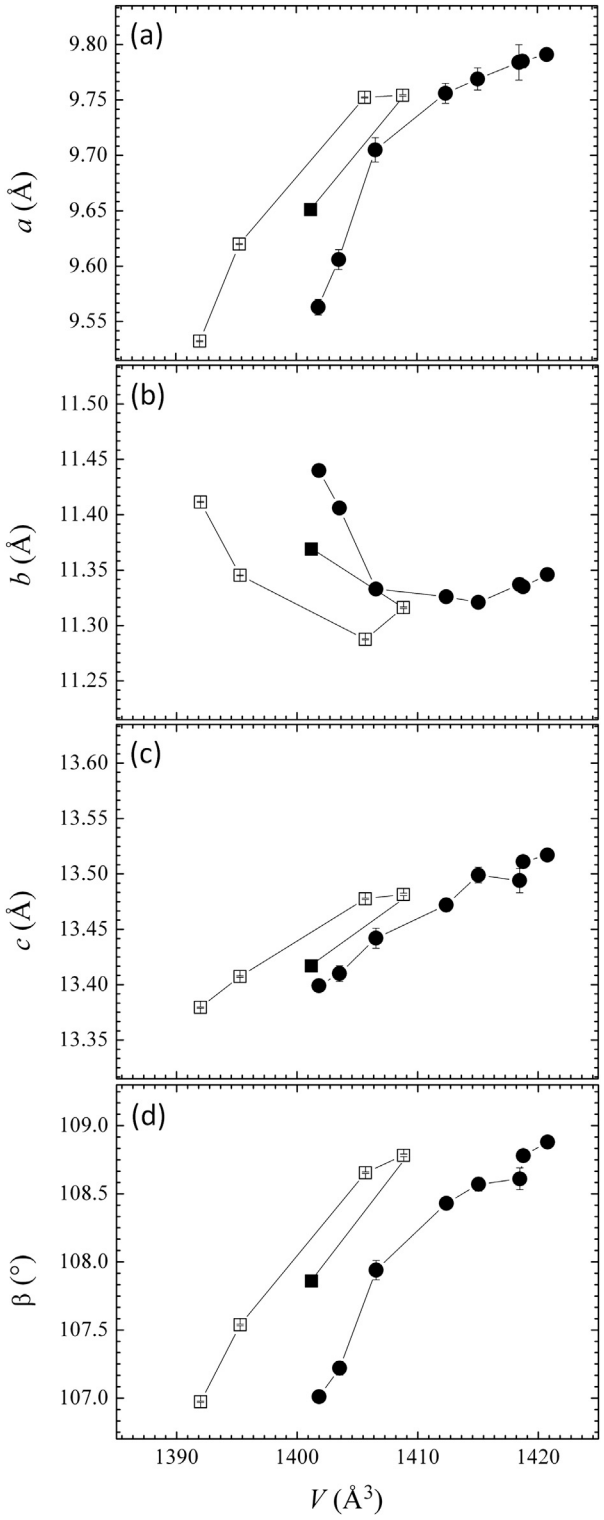

Fig. 2. Unit-cell parameters *a*, *b*, *c* (Å), and *β* (°), vs. volume variation (Å^3) of the crystal A (full circles) and the crystal B (empty squares) measured at different steps of the transformation induced by exposure to filtered visible light (>440-nm). Full square shows the apparent contraction observed after keeping the crystal B in the dark (46 days).

2.3. Raman spectroscopy

Raman spectra in the region from 80 to 1200 cm^{-1} were collected on the surface of a third crystal (C) using a confocal Raman microprobe (Horiba Jobin-Yvon LabRam-IR) coupled with an optical microscope, a HeNe laser source ($\lambda_0 = 632.8$ nm), a monochromator with holographic notch filter, a spectrometer with diffraction grating of 1800 gr/mm, and a Peltier cooled CCD detector (1024 × 256 pixels). For the purpose of this experiment the diameter of the laser spot on the sample surface was ~1 μm for the fully focused laser beam at 100× objective magnification, the beam power employed was ~2 mW. The spectral resolution was 1 cm^{-1} and the instrument was calibrated against the Stokes Raman signal

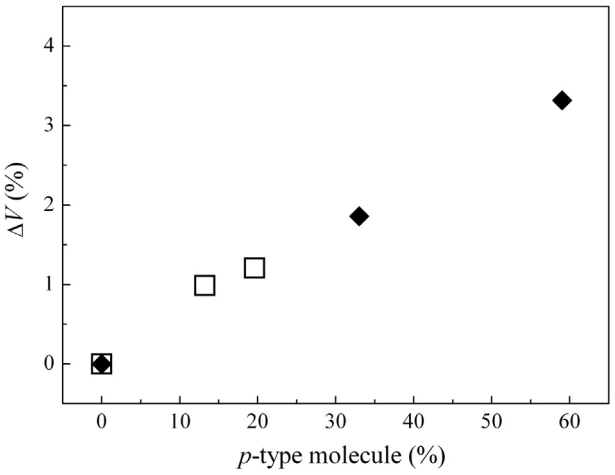

Fig. 3. Relative variation of unit-cell volume vs. the percentage of the *p*-type molecule replacing the *r*-type molecule in the $(HgBr_2)_3(As_4S_4)_2$ (empty squares; this study) and $(HgI_2)(As_4S_4)$ (black diamonds [17]).

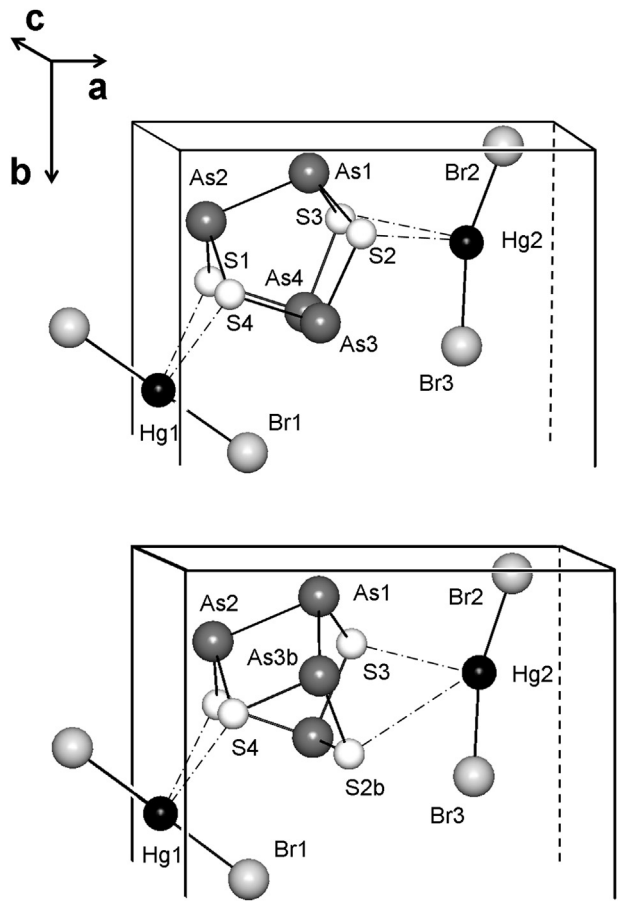

Fig. 4. Structural detail of $(HgBr_2)_3(As_4S_4)_2$ (asymmetric unit) showing the Hg–S interactions occurring between the $HgBr_2$ groups and the *r*-type As_4S_4 molecule in the non altered adduct (upper drawing) and the *p*-type As_4S_4 molecule in the compound after 420 min of light exposure (lower drawing). (The coexistent *r*-type As_4S_4 molecule, which is still the dominant cage, is not shown for the sake of drawing readability.)

of pure Si at 520 cm^{-1} using a silicon wafer. The second order bands were not analyzed. Instrument control and data acquisition, as well as the processing and analysis of Raman spectra, were performed with the software LabSpec 5 (Horiba Jobin-Yvon). Crystal C was laid

Table 4
Selected interatomic distances (Å) for the crystal B of $(HgBr_2)_3(As_4S_4)_2$ at different times of light exposure.

	(a)	(b)	(c)	(d)	(e)
Linear $HgBr_2$ molecule					
Hg1–Br1 (x2)	2.459(1)	2.453(1)	2.441(2)	2.437(2)	2.437(7)
Bended $HgBr_2$ molecule					
Hg2–Br2	2.410(2)	2.403(2)	2.403(2)	2.400(2)	2.401(8)
Hg2–Br3	2.418(2)	2.407(2)	2.396(2)	2.393(3)	2.402(8)
Br2–Hg2–Br3	161.60(7)	162.58(6)	165.10(9)	165.7(1)	163.2(3)
***r*-type molecule**					
As1–S2	2.249(4)	2.258(3)	2.265(5)	2.262(6)	2.25(2)
As1–S3	2.239(3)	2.246(3)	2.235(5)	2.239(5)	2.23(2)
As1–As2	2.555(2)	2.553(2)	2.545(3)	2.544(3)	2.56(1)
As2–S1	2.236(3)	2.239(3)	2.244(4)	2.240(5)	2.22(2)
As2–S4	2.242(4)	2.246(3)	2.250(5)	2.232(6)	2.21(2)
As2–As2	2.555(2)	2.553(2)	2.545(3)	2.544(3)	2.56(1)
As3–S2	2.234(4)	2.230(3)	2.229(5)	2.224(6)	2.25(2)
As3–S4	2.230(4)	2.246(3)	2.268(6)	2.296(6)	2.26(2)
As3–As4	2.576(2)	2.576(2)	2.603(3)	2.614(3)	2.59(2)
As4–S1	2.241(4)	2.237(3)	2.226(5)	2.227(5)	2.24(2)
As4–S3	2.246(4)	2.241(3)	2.248(5)	2.244(5)	2.25(2)
As4–As4	2.576(2)	2.576(2)	2.603(3)	2.614(3)	2.59(2)
***p*-type molecule**					
As1–S3			2.235(5)	2.239(5)	
As1–As2			2.545(3)	2.544(3)	
As1–As3b			2.43(2)	2.44(1)	
As2–S1			2.244(4)	2.240(5)	
As2–S4			2.250(5)	2.232(6)	
As2–As1			2.545(3)	2.544(3)	
As3b–S4			2.09(2)	2.08(1)	
As3b–S2b			2.28(5)	2.49(7)	
As3b–As1			2.43(2)	2.44(1)	
As4–S3			2.248(5)	2.244(5)	
As4–S2b			2.13(5)	2.10(6)	
As4–S1			2.226(5)	2.227(5)	
As4b–S3				2.17(5)	
Shorter Hg–S intermolecular distances					
Hg1–S1	3.135(3)	3.149(3)	3.181(4)	3.194(5)	3.19(2)
Hg1–S4	3.107(4)	3.119(3)	3.164(5)	3.185(6)	3.11(2)
Hg2–S2	3.152(4)	3.192(3)	3.261(5)	3.255(6)	3.23(2)
Hg2–S3	3.063(4)	3.069(3)	3.087(5)	3.102(5)	3.10(2)

Notes: (a) = unaltered crystal; (b, c, d) = crystal exposed to filtered light (>440 nm) for 180, 420, and 600 min, respectively; (e) = crystal kept in the dark (46 days) after light-induced alteration.

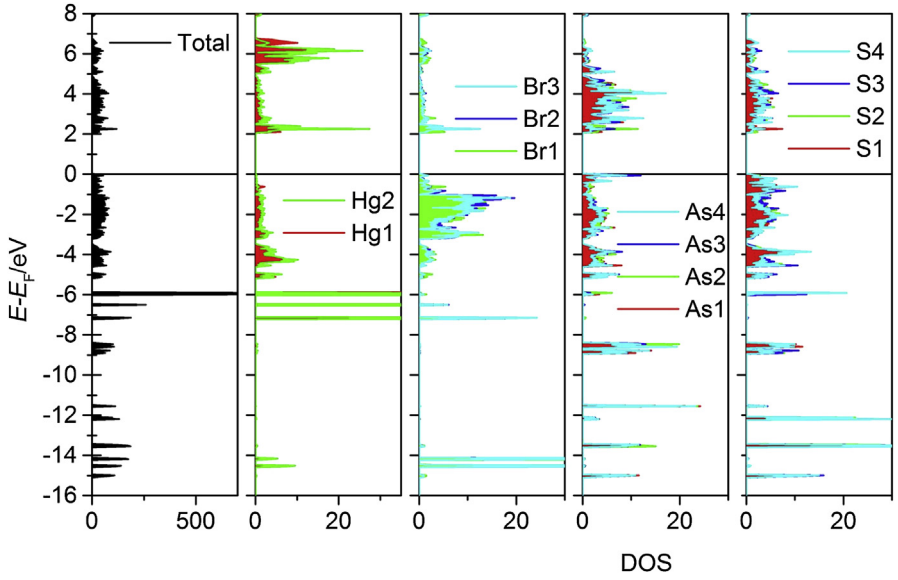

Fig. 5. Calculated atomic site projected density of states (relativistic DFG-GGA-calculations). The highest occupied states are mainly formed by As 4*p* and S 3*p* orbitals.

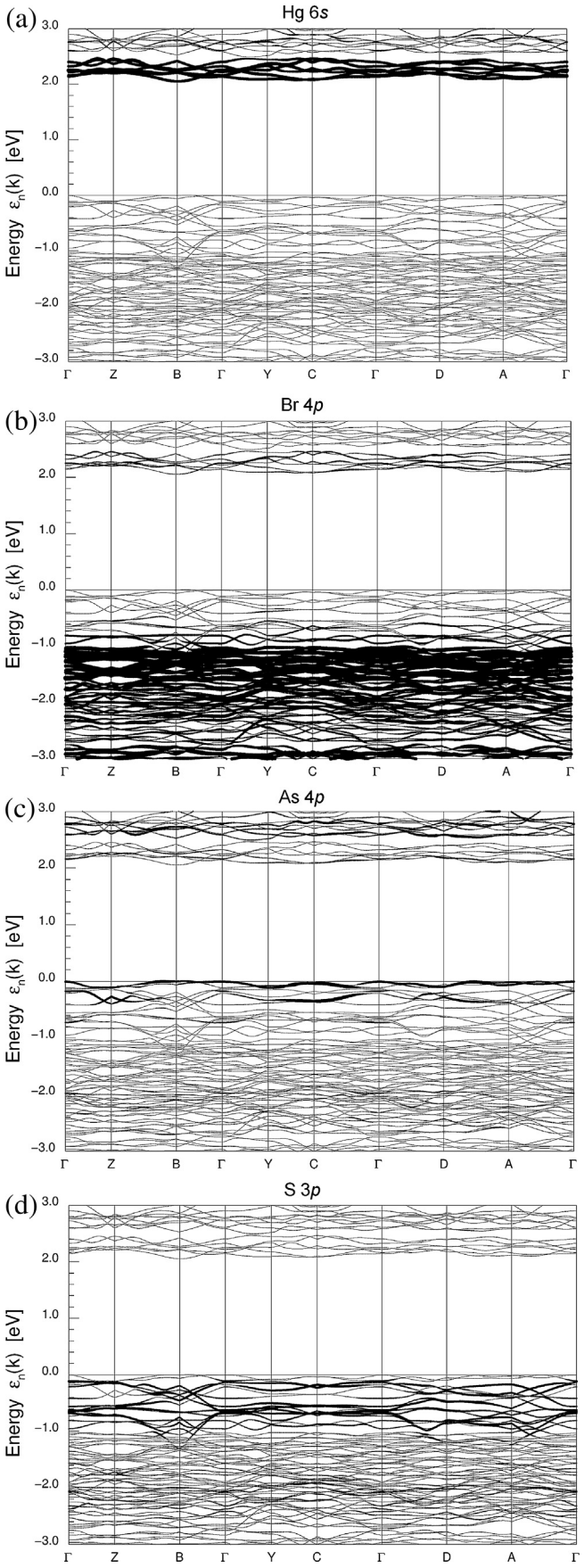

on the still support pointing the laser beam on the surface of the crystal. Spectra were acquired with an integration time of 4 s, for 6 accumulation cycles, with slit and hole aperture of 200 μm, grating of 1800 gr/mm on the unaltered crystal and every 5 min of light exposure (up to 35 min) using the 440 nm long-wavelength pass filter.

2.4. Ab initio calculations

The electronic band structure calculations were performed with the full potential local orbital code FPLO9 [25]. Therein, extended all electron basis sets include Hg-5*s*5*p*5*d*6*s*6*p*6*d*7*s*, As-and Br-3*s*3*p*3*d*4*s*4*p*4*d*5*s*5*p*, and S-2*s*2*p*3*s*3*p*3*d*4*s*4*p* valence states. Density functional theory was applied within the generalized gradient approximation (GGA [26]) in the scalar relativistic mode as described recently [27]. The calculations converged at a grid of $4 \times 4 \times 4$ *k*-points. Orbital contributions to the electronic states are analysed with respect to energy intervals (atomic site projected density of states) and *k*-points (fat band projection).

3. Results and discussion

3.1. Raman spectroscopy

The Raman spectrum collected on the unaltered crystal (n.a.) shows some very strong bands, at 182(±1), 188(±1), 195(±1), 223(±1), and 356(±1) cm^{-1}, and minor bands at 162(±1) and 146(±1) cm^{-1}, that correspond to the characteristic vibrational frequencies of the adduct $(HgBr_2)_3(As_4S_4)_2$ [20]. As the time of light-exposure increases, the pattern undergoes a clear change, the major vibrational modes of the *p*-type molecule of pararealgar [28], at 156(±1), 234(±1), and 272(±1) cm^{-1} gradually appear, and the intensities of the bands of the adduct gradually decrease (Fig. 1). Simultaneously, it can be noticed a broadening of the bands due to the progressive loss of crystallinity as well as to the superimposition of the minor bands of pararealgar at about 172, 205, 334 and 347 cm^{-1}. A slight shift of the position of the bands is due to the variations of the bond distances and bond angles caused by *p*-type molecule replacing in the lattice. As a consequence of light exposure, the colour of the crystal changed from light yellow (transparent) to brownish-yellow (opaque) after the light-induced alteration.

3.2. X-ray diffraction

The action of the light on the crystal A, employing the 550 nm long-wavelength pass filter for a maximum of 420 min, did not produce any evident effect on the unit-cell (Table 1). Differently, employing the 440 nm long-wavelength pass filter, remarkable variations of the unit-cell parameters were observed (Table 1) just after the first step (60 min) of light exposure. An increase of the *a*, *c*, and β, and a decrease of the *b* parameter, producing on the whole an expansion of the unit-cell volume, is observed as a function of the light exposure times. As shown in Fig. 2, an anisotropic unit-cell volume expansion is evident for both crystals; moreover, an apparent inversion of the trend of the lattice parameters is observed for the crystal B which was kept in dark (46 days) after the light-induced alteration. This apparent unit-cell volume contraction is analogous to that described for $(HgI_2)(As_4S_4)$ [17] where, after the loss of the crystallinity, only the core of the crystal, less

Fig. 6. Electronic band structure from a relativistic DFT-GGA calculation; orbital contributions of Hg-6*s* (a), Br-4*p* (b), As-4*p* (c), and *S*-3*p* (d) as projected onto bands are pointed out by thick lines (fat bands).

altered and with smaller unit-cell volume, contributes to the diffraction effects. In the present case no microcrystalline phases were detected after the dark stage. This implies that the outer part of the crystal turned completely amorphous, and that, being the Mo*Kα* X-ray radiation more penetrating than visible light, the *r*-type → *p*-type conversion affects only fairly the core crystal.

Structure refinements performed after different exposure times indicated the coexistence of two kinds of cage-like molecules. The first one is identical to the As_4S_4 molecule found in the structure of both realgar and β-phase [3,4], where each As atom links one As and two S atoms. The other molecule (derived from the *r*-type molecule by removing one S atom and adding another S atom in one of the two available among the six As–As edges of the As_4 disphenoidic group) is chemically and structurally identical to the molecule (*p*-type) found in pararealgar [6] and in the synthetic As_4S_4-II phase [29]. At the first step (180 min) of light-exposure (Table 2, column b), although a slight expansion of the unit-cell volume indicated possible alteration, the examination of the Δ*F*-Fourier map did not reveal the presence of any significant residual peak. Differently, after 420 min of exposure to light (Table 2, column c), the analysis of the connection between As and S atoms, including those partially occupied, suggested the coexistence of *r*-type (87%) and *p*-type (13%) As_4S_4 molecules. With the increase of the light-exposure time (Table 2, column d), the percentage of that *p*-type molecule increased up to 15% while a further disorder involving another As atom (As4–As4b split) was supposed to be the evidence of a newly formed *p*-type molecule (4%) with a different orientation, even if no evidence of residual peaks to be assigned to a corresponding new S positions was detected. Thus, at the stage (d) the total amount of *p*-type replacing *r*-type molecules was estimated to be about 20%. This last value, although affected by considerable uncertainty due the low quality of the diffraction data at this step, appears to account the relative increase of the unit-cell volume (Fig. 3), in keeping with what verified for $(HgI_2)(As_4S_4)$ [17], where the formation of a greater amount of *p*-type molecules, as much as 59%, causes a more pronounced unit-cell expansion.

In the models including both *r*-type and *p*-type As_4S_4 molecules some bond distances within the *p*-type molecule (*i.e.* As3b–S4 and As4–S2b) deviate slightly from the expected values. This is likely due to the fact that S4 and As4 are average positions for both the dominant *r*-type molecule and the less abundant *p*-type molecule. On the other hand, the $HgBr_2$ molecules are only slightly affected by the increase of the *p*-type replacing the *r*-type molecules. In particular, the <Hg–Br> bond distances become shorter (from 2.459 down to 2.437 Å and from 2.414 to 2.397 Å for Hg1 and Hg2, respectively) and the Br2–Hg2–Br3 angle increases from 161.6 to 165.7° after 600 min of light exposure. Indeed, with the decrement of S at the S2 site occurring with the *r*-type → *p*-type conversion, the Hg2–S2 interaction becomes weaker (Hg2–S2 ranging from to 3.152 to 3.255 Å after 600 min of exposure to light) in spite of the increase of the Br2–Hg2–Br3 angle (Fig. 4). In keeping with the general increase of the unit-cell volume, and similarly to what observed in the $(HgI_2)(As_4S_4)$ adduct [17], the intermolecular distances between the $HgBr_2$ groups and the *r*-type As_4S_4 cages become longer. On the contrary, couples of adjacent (if any) *p*-type molecules exhibit a stronger link via the sulphur atom at S2b position (S2b–S2b = 3.35 and 3.20 Å after light-exposure of 420 and 600 min, respectively), which well accounts for the contraction along the ***b*** axis occurring with light-induced alteration. The inversion of the trend to decrease for the *b* parameter observed between 420 and 600 min of light exposure, is probably related to the formation of a differently oriented *p*-type molecule whose formation involves moving of sulphur from the S1 site to another, not determined, S1b position. It is worth noticing that, in a *r*-type molecule, all the S atoms are equally linked to two As atoms and thus, in principle, should be all equally candidates to break the two As–S bonds. Nonetheless, we observed migration of sulphur mainly from the S2 site and, to a lesser extent, from S1. Indeed, if the shorter intermolecular contacts are taken into account (Hg–S distances in Table 4), S2 and, to a lesser extent, S1 exhibit a weaker bond with Hg (3.152 and 3.135 Å, respectively). Analogously, in the case of the $(HgI_2)(As_4S_4)$ adduct [17], the S atom 'moving' from the *r*-type molecule, is S2, which is even not bonded to Hg (Hg–S2 = 4.834 Å). The different crystal-chemical environment of the S atom implied in the molecular transformation, which is bonded to two As atoms in the $(HgI_2)(As_4S_4)$ adduct but to two As and one Hg in the structure of $(HgBr_2)_3(As_4S_4)_2$, could be the reason of the different spectral range of visible light (>550 or >440 nm, respectively) required to activate the reaction.

3.3. Electronic band structure calculations

Due to relativistic DFT-GGA band structure calculations $(HgBr_2)_3(As_4S_4)_2$ is a semiconductor with a direct band gap of 2.04 eV. The electronic density of states (DOS, Fig. 5) and the electronic band structure (Fig. 6) show flat valence (VB) and conduction bands (CB) that are due to localized covalent states within the molecular units As_4S_4 and $HgBr_2$, respectively. The analyses of orbital contributions to the band edges from atomic site projected densities of states (Fig. 5) and fat bands (Fig. 6) reveal significant differences for CB and VB that explain the observed experimental behaviour. The CB and the lowest unoccupied states (CB minimum) are mainly attributed to antibonding states of the Hg–Br bonds (Fig. 6a and b). The VB is formed by As-4*p* (Fig. 6c) and S-3*p* (Fig. 6d) states, while the highest occupied states (VB maximum) are due to non-bonding As-4*p* states. The latter also contribute to the conduction band with maxima at the region above the Hg-6*s* states (>2.5 eV). One can now draw conclusions on the experimental observations. An electronic excitation with visible light of $\lambda > 550$ nm does not affect the molecular entities as the electrons are shifted from As to Hg states, i.e. from As_4S_4 to $HgBr_2$ entities (intermolecular excitation). By contrast, a wavelength of $\lambda > 440$ nm has obviously the right energy to accelerate electrons from the bands close to the VB maximum, *i.e.* from non-bonding As-*p* states to the CB. This allows for an intramolecular excitation that causes the observed rearrangement. Therefore, it seems quite reasonable to attribute the structural changes of the As_4S_4 cage molecules to a light-induced bond-cleavage and rearrangement. The $HgBr_2$ molecules are not affected by light of this wavelength since the corresponding states are lying much lower in energy.

Acknowledgements

This work was funded by M.I.U.R.-P.R.I.N. 2009 entitled "Modularity, microstructures and non-stoichiometry in minerals" to P. Bonazzi.

References

[1] R. Holomb, V. Mitsa, P. Johansson, N. Mateleshko, A. Matic, M. Veresh, Chalcogenide Lett. 2 (2005) 63–69.
[2] P. Němec, J. Jedelský, M. Frumar, Z. Černošek, M. Vlček, J. Non-Crystal. Solids 351 (2005) 3497–3502.
[3] D.J.E. Mullen, W. Nowacki, Z. Kristallogr. 136 (1972) 48–65.
[4] E.J. Porter, G.M. Sheldrick, J. Am. Chem. Soc. Dalton 13 (1972) 1347–1349.
[5] A.C. Roberts, H.G. Ansell, M. Bonardi, Can. Mineral. 18 (1980) 525–527.
[6] P. Bonazzi, S. Menchetti, G. Pratesi, Am. Mineral. 80 (1995) 400–403.
[7] D.L. Douglass, C. Shing, G. Wang, Am. Mineral. 77 (1992) 1266–1274.
[8] P. Bonazzi, S. Menchetti, G. Pratesi, M. Muniz-Miranda, G. Sbrana, Am. Mineral. 81 (1996) 874–880.
[9] A. Kyono, M. Kimata, T. Hatta, Am. Mineral. 90 (2005) 1563–1570.
[10] P. Ballirano, A. Maras, Eur. J. Mineral. 18 (2006) 589–599.

[11] P. Bonazzi, L. Bindi, G. Pratesi, S. Menchetti, Am. Mineral. 91 (2006) 1323–1330.
[12] A. Kyono, J. Photochem. Photobiol. A Chem. 189 (2007) 15–22.
[13] P. Naumov, P. Makreski, G. Jovanovski, Inorg. Chem. 46 (2007) 10624–10631.
[14] P. Naumov, G. Petruševski, T. Runčevski, G. Jovanovski, J. Am. Chem. Soc. 132 (2010) 11398–11401.
[15] M. Zoppi, G. Pratesi, Am. Mineral. 97 (2012) 890–896.
[16] L. Bindi, V. Popova, P. Bonazzi, Can. Mineral. 41 (2003) 1463–1468.
[17] P. Bonazzi, L. Bindi, M. Muniz-Miranda, L. Chelazzi, T. Rödl, A. Pfitzner, Am. Mineral. 96 (2011) 646–653.
[18] M.F. Bräu, A. Pfitzner, Angew. Chem. Int. Ed. 45 (2006) 4464–4467.
[19] P. Bonazzi, L. Bindi, Z. Kristallogr. 223 (2008) 132–147.
[20] M.F. Bräu, A. Pfitzner, Z. Anorg. Allg. Chem. 633 (2007) 935–937.
[21] P. Bonazzi, L. Bindi, V. Popova, G. Pratesi, S. Menchetti, Am. Mineral. 88 (2003) 1796–1800.
[22] Oxford Diffraction, CrysAlis RED (Version 1.171.31.2) and ABSPACK in CrysAlis RED, Oxford Diffraction Ltd, Abingdon, Oxfordshire, England, 2006.
[23] G.M. Sheldrick, Acta Crystallogr. A64 (2008) 112–122.
[24] J.A. Ibers, W.C. Hamilton (Eds.), International Tables for X-ray Crystallography, vol. IV, Kynock, Dordrecht, The Netherlands, 1974, p. 366.
[25] K. Koepernik, H. Eschrig, Phys. Rev. B 59 (1999) 1743–1757.
[26] J.P. Perdew, K. Burke, M. Ernzerhof, Phys. Rev. Lett. 77 (1996) 3865–3868.
[27] J. Rothballer, F. Bachhuber, F. Pielnhofer, F.M. Schappacher, R. Pöttgen, R. Weihrich, Eur. J. Inorg. Chem. 2 (2013) 248–255.
[28] M. Muniz-Miranda, G. Sbrana, P. Bonazzi, S. Menchetti, G. Pratesi, Spectr. Acta A52 (1996) 1391–1401.
[29] V.A. Kutoglu, Z. Anorg. Allg. Chem. 419 (1976) 176–184.